Journal of Materials Chemistry

Dynamic Article Links

Cite this: J. Mater. Chem., 2012, 22, 12666

www.rsc.org/materials

PAPER

Photocatalytic cellulosic electrospun fibers for the degradation of potent cyanobacteria toxin microcystin-LR†

Nicholas M. Bedford,[ab] Miguel Pelaez,[c] Changseok Han,[c] Dionysios D. Dionysiou[c] and Andrew J. Steckl*[ad]

Received 14th March 2012, Accepted 9th May 2012
DOI: 10.1039/c2jm31597a

Non-woven, high surface area photocatalytic cellulosic electrospun fibers were fabricated for solar-light-driven water treatment purposes and tested for photocatalytic decomposition of the potent cyanobacteria toxin microcystin-LR (MC-LR). Electrospun fibers of cellulose acetate were converted to succinylated cellulose and then loaded with titania nanoparticles using a simple solution based technique. It was found that the type of titania nanoparticle (visible light activated or UV light activated), the surface area of the fiber mat, and loading solution pH all have an effect on the distribution of titania along the fibers. The titania coverage and surface area of the fiber mats were found to correlate well with the degree of MC-LR degradation under both visible and solar light irradiation. The difference in titania coverage, determined using X-ray photoelectron microscopy (XPS), was two to three times smaller in the lower surface area samples. These photocatalytic electrospun fibers could be advantageously used for drinking water and wastewater treatment applications using solar light as a renewable source of energy.

Introduction

The need for low cost and efficient water treatment strategies is an ever increasing necessity given various sources of pollution attributed from industrial and natural sources.[1–6] Solar light driven photocatalysis with nanoparticles (such as titania, TiO_2) show tremendous promise as a simple and energy efficient technology for water purification and treatment.[7,8] Metal oxide photocatalysts readily generate hydroxyl and oxygen radicals upon exposure to light exceeding the band gap energy which can degrade organic contaminants at the surface of the photocatalyst.[9] The titania nanoparticle variant P-25, in particular, exhibits the highest photocatalytic degradation of most organic contaminants of the commercially available metal oxide photocatalysts. This is due to longer charge-pair recombination lifetime and faster interfacial charge transfer rate.[9] Titania is also a fairly inexpensive nanomaterial and is chemically stable, thus allowing it to be implemented in a wide variety of applications.[10–15]

The controlled immobilization of titania nanoparticles is a major obstacle in the successful use of these materials for water purification. Nanoscale titania particles are difficult to recover from free suspensions due to their intrinsically small sizes. Simple immobilization of the photocatalytic materials onto conventional substrates reduces the available surface area due to the interactions between the photocatalyst and substrate, limiting the rate of photocatalytic activity. Another issue with more common variants of titania is the inefficient absorption of the solar spectrum as these nanoparticles typically only absorb UV light. This only encompasses ~5% of the solar spectrum, which limits the amount of available sunlight that can be used for photocatalysis. To circumvent this issue, methods have been developed to extend the photon absorption properties of titania into the visible light region of the solar spectrum. These include dye sensitization[16–18] and doping with metal[19–21] and non-metal[22–29] elements. In water treatment applications, the use of dyes and metal dopants are not suitable for long term usage due to potential leaching of these materials from the photocatalyst, which could pose serious environmental and health issues. Doping with non-metal elements, such as carbon, nitrogen, fluorine, and sulfur, serves as an environmentally benign alternative to increase the photon collecting efficiency of solar light driven photocatalyst in titania.

The immobilization of titania onto a membrane-like substrate is of interest in water treatment applications as it could circumvent issues associated with using nanoparticle colloids and could still potentially have a high surface area to volume ratio. Furthermore, if the substrate was from a biodegradable, renewable and inexpensive source it would have added environmental and

[a]Nanoelectronics Laboratory, University of Cincinnati, Cincinnati, OH, 45221, USA. E-mail: a.steckl@uc.edu
[b]Materials Engineering Program, School of Energy, Environmental, Biological and Medical Engineering, University of Cincinnati, Cincinnati, OH, 45221, USA
[c]Environmental Engineering and Science Program, School of Energy, Environmental, Biological and Medical Engineering, University of Cincinnati, Cincinnati, OH, 45221, USA
[d]Electrical Engineering Program, School of Electronic and Computing Systems, University of Cincinnati, Cincinnati, OH, 45221, USA
† Electronic supplementary information (ESI) available. See DOI: 10.1039/c2jm31597a

economical benefits. Cellulosic materials could serve as environmentally friendly substrate candidates for titania given the low cost, biodegradable/renewable and chemical robustness of these materials.[30] Cellulosic materials can be modified with the appropriate functionalities to have higher affinity for titania nanoparticles. Titania based photocatalytic textile-like materials could also be useful in other applications, such as protective/self-cleaning clothing. Various groups have reported on the use of commercially available cellulosic textiles as substrates for titania.[31–33] An issue with these substrates is a relatively low surface area to volume ratio given the large fiber diameter used in commercial textiles. Non-woven three-dimensional meshes containing nano and sub-micron sized fibers can be easily obtained using the electrostatic fiber deposition process known as electrospinning.[34,35] Electrospun photocatalytic fibers have been previously made from titania sol/polymeric fibers (which after calcination yields pure titania),[36–38] electrospun polymeric fibers with layer-by-layer assembly of titania nanoparticles post-electrospinning,[39,40] and by coaxial electrospinning.[41]

In this study, we report on the use of photocatalytic cellulosic non-woven nanofiber mats created by electrospinning for the degradation of the potent toxin microcystin-LR (MC-LR). MC-LR is one of the most commonly found cyanobacteria toxins generated by the more frequently occurring cyanobacteria algae blooms in various water sources across the world. The toxin natural proximity to drinking water sources, high water solubility, modest chemical stability, and high hepatotoxicity have made MC-LR contaminated water a serious health risk.[42,43] To address this problem, high surface area photocatalytic cellulosic fibers are formed by first electrospinning solutions of cellulose acetate (CA) into non-woven fiber meshes. The CA fibers are then converted to succinylated cellulose fibers through a series of simple reactions. Next, the succinylated fibers are loaded with titania from aqueous dispersions. Visible light activated titania is used to absorb a larger portion of the solar spectrum. The fiber mats' surface area, and titania surface coverage, were found to have the most dramatic effect on the overall MC-LR degradation. These high surface area non-woven photocatalytic mats can effectively degrade MC-LR and show promise for photocatalytic drinking water treatment using solar light.

Experimental

Electrospinning

Solutions of cellulose acetate (CA, 39.8% acetyl content, M_w = 30 000 g mol^{-1}, purchased from Sigma-Aldrich) were made in 90% and 80% acetic acid (aq) at a concentration of 17 wt%.[44] Electrospinning was performed using a variable high voltage power supply (Glassman High Voltage) operating at 25 kV using a 5 × 5 cm Al collecting plate. CA solutions were fed to a spinneret (18 gauge blunt needle) at a flow rate of 0.5–0.6 mL h^{-1} using a syringe pump (Stoelting Co.). The spinneret to substrate distance was set to 11 cm for all experiments. All electrospinning experiments were performed under ambient conditions.

Fiber processing

CA fibers were deacetylated to cellulose using 0.5 N KOH in ethanol, as described previously.[41] After 30 min, the cellulose fibers were removed from the ethanol solution and placed in 0.5 N HCl, followed by neutralization using 0.5 N KOH (aq). The fiber mats were washed in distilled water and dried under ambient conditions. The fibers were then placed in a 10% (w/v) succinic anhydride in dimethylformamide (DMF) solution for succinylation of the hydroxyl groups for two hours at 65 °C.[45] The succinylated cellulose fibers were then washed extensively with DMF to remove any un-reacted succinic anhydride and then washed with water to remove the DMF. Finally, the samples were loaded with 1 wt% titania nanoparticle dispersions (sonicated with a probe ultrasonicator prior to loading) at acidic (pH = 2), near-neutral (pH = 6), and basic (pH = 10) pH for one hour at 75 °C. Acidic and basic solutions were made with HCl and KOH respectively. Titania dispersions consisted of P-25 (Degussa Aeroxide, purchased from Acros Organics), visible light activated Kronos vpl 7000 (purchased from Kronos Worldwide Inc., herein referred to only as Kronos), or nitrogen and fluorine doped titania (NF–TiO_2) made by sol–gel techniques. NF–TiO_2 synthesis details can be found elsewhere.[23] Titania loaded fiber samples were sonicated in distilled water immediately after loading to remove any unbound titania.

Photocatalytic degradation of MC-LR

For the photocatalytic evaluation of the electrospun fibers, double distilled water (pH 5.7) was spiked with an aliquot of MC-LR standard (Calbiochem) to achieve an initial concentration of 500 ± 20 μg L^{-1} of MC-LR. Each fiber mat was weighed (~25 mg) and introduced to a glass reactor (I.D. 4.7 cm) that contains the previously spiked solution. A solar simulator (Newport Corporation) equipped with a 300 W Xe lamp, atmospheric attenuation (AM 1.5) and an infrared (IR) blocking filter was introduced. To obtain visible light irradiation only, an additional UV-block filter was included in the set up. The average light intensity reaching the reactor was 25 mW cm^{-2} for the visible range as measured by a broad band radiant power meter (Newport Corporation). For the experiments under solar irradiation, the UV-block filter was removed and the average light intensity was 47.1 mW cm^{-2}. For reference, the intensity of sunlight at earth's surface is approximately 100 mW cm^{-2}.[46] The reactor was sealed and cooled down with a fan to prevent evaporation during irradiation. Adsorption experiments were carried out under dark conditions to account for MC-LR absorption onto the photocatalytic fibers. Samples were obtained at established times and the concentration of MC-LR was determined by liquid chromatography according to Antoniou *et al.*[47] A slight variation to the analytical method was done by introducing a C18 Discovery (Supelco) column with 2.1 μm particle size in order to reduce the flow rate to 0.2 mL min^{-1} and the injection volume to 20 μL.

Characterization

Fiber morphology was studied using a FEI/Phillips XL30 field-emission environmental scanning electron microscope (FE-ESEM). Average fiber diameter calculations were performed by taking 20+ line scans over several SEM images. Chemical modification of cellulosic fibers was characterized using a Thermo Scientific Nicolet 6700 infrared (IR) spectrometer

operating in transmission mode. BET analysis of succinylated cellulose fiber meshes were performed with a Tristar 3000 (Micromeritics) porosimeter analyzer. The samples were vacuum freeze-dried (Labconco) for 24 h before analysis. X-ray photoelectron spectroscopy (XPS) was performed using an M-Probe Surface Spectrometer (Surface Science) to determine the surface Ti/C ratio on the fiber samples. A total of three photocatalytic fiber meshes were analyzed in three different areas to obtain an average surface Ti/C ratio. Ti-assay experiments were performed using a modified method from Sedaira *et al.*[48] Briefly, fiber samples were dissolved in 50% (w/v) ammonium sulfate in concentrated sulfuric acid at ~100°C. 100 μL of the digested material was then added to 20 mL of 0.3125% (w/v) 5-chlorosalicylic acid, 0.125 M $NaClO_4$ in 50 : 50 water–ethanol, adjusted to pH = 3 (±0.1) with concentrated ammonium hydroxide, and diluted to 25 mL with water. The quantification of Ti was performed by measuring the absorption of the solution at 355 nm. A standard solution of Ti was made by dissolving titania nanoparticles in 50% (w/v) ammonium sulfate in concentrated sulfuric acid to obtain a calibration curve. Each sample tested was analyzed in triplicate. In order to obtain the size distribution of titania particles, dynamic light scattering (DLS) was performed by ALV/CGS-3 using a 22 mW HeNe laser operating at 632.8 nm with a data acquisition time of 30 s. Nanoparticle dispersions were tested immediately after probe sonication.

Results and discussion

To determine the effect of available surface area on photocatalytic performance, the electrospun fiber diameter was varied by changing the amount of acetic acid in the electrospinning solution as previously reported.[44] Fibers electrospun from a 17 wt% solutions of 80% and 90% acetic acid (aq) are shown in Fig. 1. Average fiber diameter and BET surface area for these samples are given in Table 1. Fibers electrospun from an 80% acetic acid solution have an average diameter of 230 ± 40 nm, while fibers electrospun from a 90% acetic acid solution have an average diameter of 320 ± 120 nm. This increase in fiber diameter and range of fiber diameter with increasing acetic acid is consistent with reported values.[44] Fibers electrospun from the 80% acetic acid solution showed an increase in BET surface area (5.6 ± 0.1 $m^2\ g^{-1}$ *vs.* 4.9 ± 0.1 $m^2\ g^{-1}$) compared to fibers electrospun from the 90% acetic acid solutions (Table 1). The CA electrospun fibers were then converted to cellulose, followed by a succinylation reaction to functionalize the cellulosic fibers with carboxylic acid groups (see Experimental section). SEM images of fibers with each of the described functionalities are shown in Fig. 2 for fibers electrospun from 80% acetic acid (aq) solutions. Conversion of the CA fibers (Fig. 2a) to cellulose fibers (Fig. 2b) and then to succinylated cellulose fibers (Fig. 2c) resulted in a slight change in overall fiber diameter and BET surface area of the fibers (Table 1). Carboxylic acid functionality was used as these groups are known to bind titania better than acetyl and hydroxyl groups found in the CA and cellulose fibers.[31,45,49] To illustrate this, identical concentrations of P-25 were loaded onto cellulose fibers and succinylated cellulose fibers as shown in Fig. 3. There is a clear difference in the amount of titania loaded onto the carboxylic acid functionalized fibers (Fig. 3a) than the hydroxyl containing cellulosic fibers (Fig. 3b). IR spectroscopy was used to confirm the conversion of the cellulosic fiber materials (Fig. S1†). The initial CA fibers have strong peaks at 1740 cm^{-1} and 1230 cm^{-1} (Fig. S1†, red line) which are associated with carbonyl stretching and ether bond stretching in the acetyl group, respectively.[50] Following deacetylation, the aforementioned peaks are absent from the spectrum (Fig. S1†, dashed black line) along with the addition of the broad peak from 3600–3000 cm^{-1} corresponding to hydroxyl groups. Upon addition of succinic acid to the hydroxyl groups of the cellulose, the carbonyl peak reappears at 1715 cm^{-1}, while maintaining the broad peak for the hydroxyl group (Fig. S1†, dashed blue line). The shift to lower absorption wavenumber from the carbonyl in the acetyl to carboxylic acid group has been shown previously.[51]

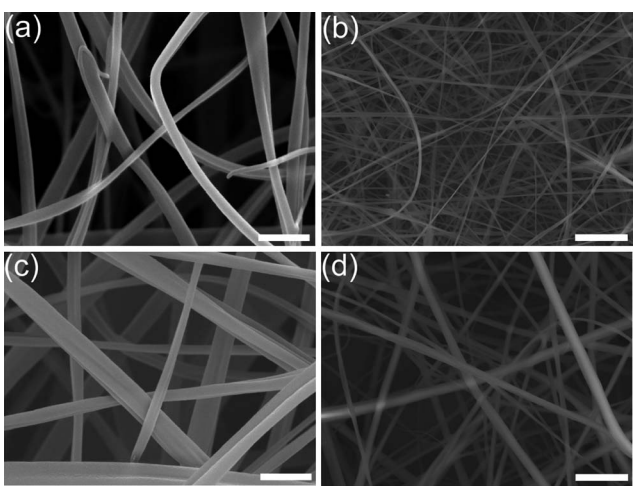

Fig. 1 FE-SEM images of CA fibers electrospun from (a) and (b) 80% acetic acid solution (aq) (1 μm and 5 μm scale bars respectively); (c) and (d) 90% acetic acid solution (aq) (1 μm and 5 μm scale bars respectively).

The electrospun fibers were loaded with three different types of titania at pH = 6 as described in the Experimental section (Fig. 4). P-25 absorbs only UV light, while Kronos titania and NF–TiO_2 display absorption spectra into the visible spectrum (out to ~600 and 500 nm, respectively). As seen in Fig. 4, the fiber coverage of the loaded titania in the cellulosic fiber mats is vastly different for the three types of titania. Kronos nanoparticles tend to form small sized clusters along the fiber (~100 nm) that are accompanied by larger spherical clusters (~1 to 3 μm) that are typically imbedded in the pores of the fiber mat. The NF-doped titania also shows smaller and larger clusters. However the larger sized clusters are much bigger than those seen in the Kronos loaded fiber samples. Furthermore, the overall amount of titania bound to the fibers appears to have decreased. Conversely, P-25 nanoparticles bind to the succinylated fibers more uniformly without the large aggregates seen in the visible light activated samples.

To obtain more quantitative information on the overall amount of titania in the fiber mats as well as the extent of titania coverage on the surface of the fibers Ti assays and XPS experiments were performed, respectively (Table 2). An example XPS spectrum can be found in Fig. S2†. The ratio of surface titanium to carbon was calculated by the atomic percentages of each element obtained from XPS. Elemental analysis from XPS shows

Table 1 Fiber diameter and BET surface area, from non-woven cellulosic fiber mat samples electrospun from varying concentrations of acetic acid

	80% Acetic acid			90% Acetic acid		
	CA	Cellulose	Succinylated cellulose	CA	Cellulose	Succinylated cellulose
Fiber diameter (nm)	230 ± 40	210 ± 40	200 ± 40	320 ± 120	380 ± 80	370 ± 70
BET surface area (m^2 g^{-1})	5.6 ± 0.1	6.10 ± 0.08	6.0 ± 0.1	4.9 ± 0.1	4.86 ± 0.05	4.63 ± 0.08

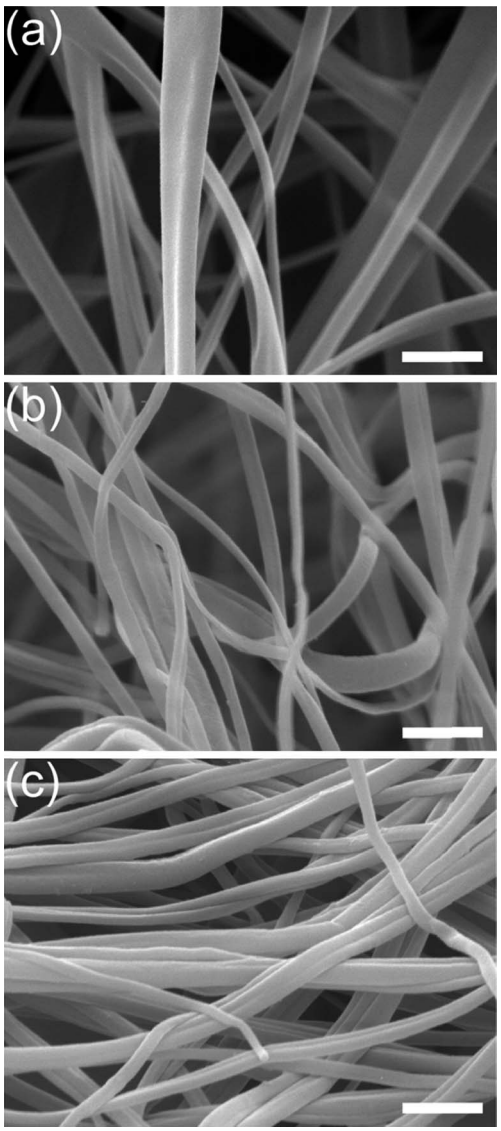

Fig. 2 FE-SEM images: (a) CA nanofibers; (b) cellulose nanofibers; (c) succinylated cellulose nanofibers. Initial CA nanofibers were electrospun from an 80% acetic acid solution (aq). All scales bars equal 1 μm.

that P-25 covers the fibers more uniformly than the visible light activated titania nanoparticles, which is consistent with FE-SEM observations. The NF-doped titania, in particular, has an order of magnitude lower surface Ti/C ratio than P-25 and Kronos, which is due to its comparatively lower dispersibility in water. This results in large aggregates observed throughout the fiber mat (Fig. 4). Fibers electrospun from an 80% acetic acid solution have a higher surface coverage of Kronos and NF-doped titania

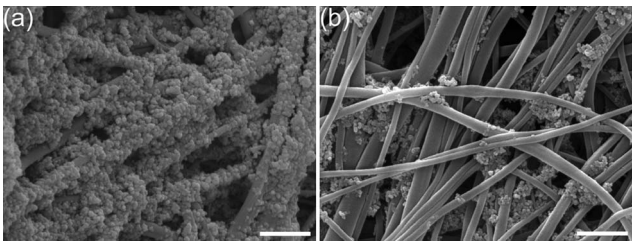

Fig. 3 FE-SEM images of P-25 loaded fibers from a 17 wt% CA solution in 80% acetic acid (aq): (a) succinylated cellulose fibers and (b) cellulose fibers (scale bar equals 2 μm). All scale bars equals 1 μm.

compared to fibers electrospun from 90% acetic acid solutions. The surface coverage of P-25 from the fiber samples is similar, which is due to the ability for P-25 to disperse better in aqueous media. Regarding the total amount of titania loaded into the fiber mats, the NF–TiO_2 generally have the higher titania percentages compared to P-25 and Kronos. However, the surface coverage is poor, with large aggregates of titania found within the fiber mat (Fig. 4), which significantly contributes to the larger overall titania percentages found in these fibers. The fibers electrospun from 90% acetic acid tend to have larger overall amounts of titania, although surface coverage of titania is less than those seen in fibers electrospun from 80% acetic acid. This is likely due to the larger surface area of these fibers, as the size titania aggregates are unchanged between the two electrospun fiber templates.

The photocatalytic degradation of MC-LR by photocatalytic cellulosic fibers loaded with titania at pH = 6 under visible and solar light is shown in Fig. 5 and 6, respectively. The extent of adsorption percentage of MC-LR onto the fiber mats is shown in Table 3. It is worth noting that the adsorption of MC-LR onto succinylated cellulose fibers without titania is much higher than fibers with titania. This is likely due to the high degree of hydrogen bonding between the succinic acid functionality on the fibers and the functional groups and peptide bonds in MC-LR. With the addition of titania, the amount of adsorbed MC-LR is reduced likely due to the decrease in free acid groups along the fiber. Under visible light irradiation (>420 nm), the Kronos and NF-doped titania show significant degradation of MC-LR while P-25 does not show any photocatalytic activity under these irradiation conditions (decrease in MC-LR concentration due to adsorption of toxin, Table 3). The Kronos loaded fiber samples degrade MC-LR faster at identical photon energies than the NF doped titania loaded fibers, despite the NF-doped titania exhibiting comparable degradation rates of MC-LR as pristine nanoparticles in solution.[23] In fibers electrospun from 80% acetic acid, the Kronos loaded fibers degrade ~40% more MC-LR over the course of experimentation than the NF–TiO_2 loaded samples.

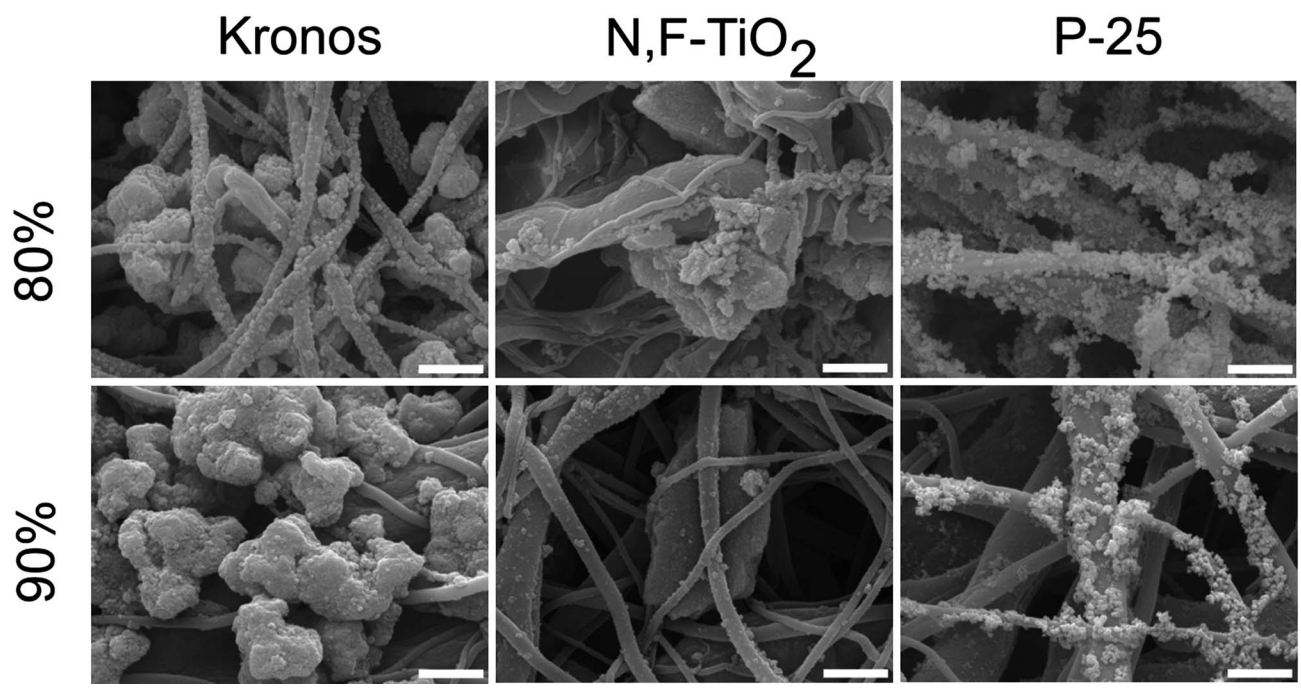

Fig. 4 FE-SEM images of titania-loaded succinylated cellulose nanofibers. Fibers are electrospun from 17 wt% CA solutions in 80% and 90% acetic acid (aq). Images are shown for fibers loaded with Kronos, NF–TiO_2 and P-25. All scale bars equal 1 μm.

Table 2 Surface Ti/C ratio (as determined using XPS) and percentage of titania in the fiber mats (as determined using a Ti-assay) for fibers electrospun at two different acetic acid concentrations and loaded with three titania variants. Each experiment was repeated three times on three separately made samples

	P-25		Kronos		NF–TiO_2	
	80%	90%	80%	90%	80%	90%
Surface Ti/C ratio	0.5 ± 0.4	0.4 ± 0.1	0.30 ± 0.05	0.10 ± 0.05	0.03 ± 0.01	0.012 ± 0.006
TiO_2%	10 ± 2%	16 ± 10%	6 ± 1%	19 ± 5%	20 ± 8%	11 ± 2%

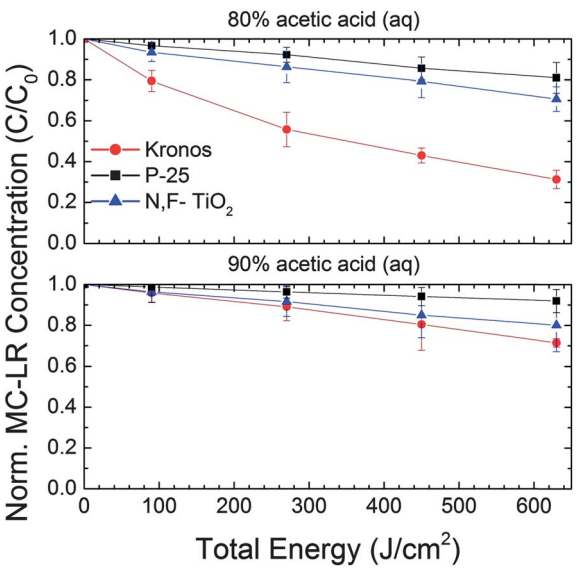

Fig. 5 Photocatalytic degradation of MC-LR under visible light conditions (average light intensity of 25 mW cm^{-2}) for Kronos loaded fibers (red circles), NF–TiO_2 loaded fibers (blue triangles), and P-25 (black squares). The top and bottom graphs correspond to fiber electrospun from 17 wt% CA solutions in 80% and 90% acetic acid (aq), respectively.

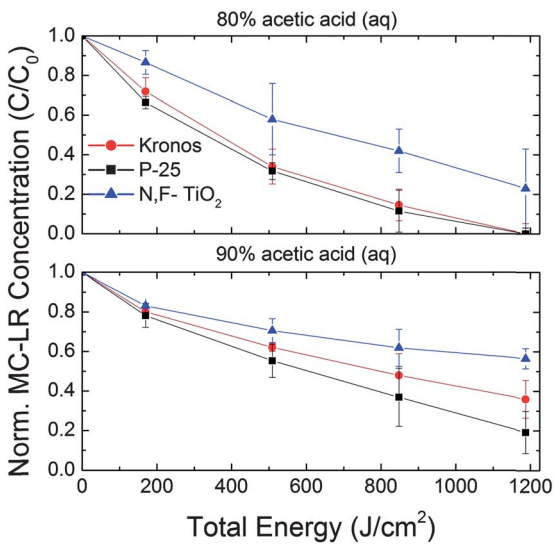

Fig. 6 Photocatalytic degradation of MC-LR under solar light conditions (average light intensity of 47.1 mW cm^{-2}) for Kronos loaded fibers (red circles), NF–TiO_2 loaded fibers (blue triangles), and P-25 (black squares). The top and bottom graphs correspond to fiber electrospun from 17 wt% CA solutions in 80% and 90% acetic acid (aq), respectively.

Table 3 Adsorption of MC-LR onto various fiber mats after 7 h as determined by taking aliquots of MC-LR from fiber samples under dark conditions

Fiber sample	NF–TiO_2 loaded	Kronos loaded	P25 loaded	No TiO_2
80% acetic acid	12.7%	13.4%	14.3%	59.1%
90% acetic acid	6.3%	6.8%	7.3%	28.7%

This difference is reduced to ~10% in fiber electrospun from 90% acetic acid solutions. Under solar light conditions, all samples tested exhibit enhanced photocatalytic activity as the titania nanoparticles absorb more light, which causes an increase the photocatalytic activity. Once again, fiber samples loaded with P-25 and Kronos degrade MC-LR faster than samples loaded with NF-doped titania. Kronos and P-25 loaded samples completely degraded MC-LR for samples electrospun from 80% acetic acid. Samples electrospun from 90% acetic acid solution exhibited comparatively lower MC-LR degradation due to the decreased surface coverage of titania and overall decrease in surface area.

While it is difficult to calculate accurate rate constants due to the heterogeneity of the samples (in terms of both chemical constituency and uniformity), certain metrics obtained from Table 2 can help explain MC-LR degradation behavior. Under visible light irradiation, the Kronos loaded samples degrade MC-LR faster than the NF–TiO_2 loaded fibers. This is due to the more uniform coverage of the Kronos on the fiber mats compared to the NF–TiO_2 despite the larger overall amount of the NF–TiO_2 in the sample. The importance of titania surface coverage is again displayed for samples tested under solar irradiation, as fibers loaded with P-25 and Kronos exhibit higher rates of MC-LR degradation compared to samples loaded with NF–TiO_2. In more general terms, fiber mats electrospun from 80% acetic acid degrade MC-LR faster than fiber mats electrospun from 90% acetic acid. The surface coverage of titania on fibers electrospun from 80% acetic acid are generally higher than for fibers electrospun from 90% acetic acid despite the fact that there is generally more titania (for P-25 and Kronos) in the 90% acetic acid samples (Table 2). This illustrates the relative importance of titania coverage and substrate surface area over the total amount of titania.

In order to increase the titania surface coverage in the photocatalytic electrospun fibers, titania aggregate sizes in the loading solution should be decreased. This was accomplished by loading titania onto the electrospun fibers at acidic and basic pH. Solutions used in the data presented up to this point have a pH of ~6, which is close to the isoelectric point (IEP) for the titania nanoparticles used in this study.[23,52] Aggregate size of titania at a pH of 2, 6, and 10 were determined using dynamic light scattering (DLS) and are given in Table 4. P-25 aggregate sizes are consistent with values reported in the literature,[52,53] with large aggregate size at pH = 6 (around P-25's IEP) and smaller aggregate sizes above and below the IEP. This decrease in aggregate size is due to electrostatic repulsion as titania becomes charged below (positive) and above (negative) the IEP. This trend is also exhibited in the NF–TiO_2 nanoparticles at larger sizes. Kronos nanoparticles exhibit a smaller average aggregate size at a pH of 2, while higher pH values lead to increased aggregate sizes.

Dispersions at varying pH values were then loaded onto succinylated cellulose fibers initially electrospun from an 80% acetic acid solution. Ti assays and XPS experiments were again used to determine the total amount of titania within the fibers mats and the TiO_2 surface coverage for samples loaded at different pH values (Table 5). The calculated Ti/C ratio from XPS data is higher at lower pH for all titania nanoparticles tested and decrease with increasing pH. The NF–TiO_2 loaded fibers exhibited the lowest Ti/C ratio of all the samples tested at pH = 6 and 10, but exhibit a larger comparative increase in Ti/C ratio at a loading pH = 2. The overall titania coverage in the electrospun fiber mats, as obtained by Ti assay experiments, was found to be comparable or slightly higher in samples loaded in acidic conditions compared to a pH = 6 (within standard deviation) and much smaller at higher pH. Titania aggregate size and surface coverage of titania on the fiber mats was observed using SEM (Fig. 7). The titania morphology within the fiber mats is consistent with data obtained from DLS and XPS.

The relative distribution and amounts of titania present in the fiber mats can be understood in terms of titania aggregate sizes as well as the surface chemistries of the nanoparticles and nanofibers at the three different pH as shown schematically in Fig. 8. At basic pH, succinic acid functionality in the electrospun fibers likely displays a carboxylate anion while the dispersed titania nanoparticles bear a negative charge.[52] At pH = 10 the electrospun fibers and the titania electrostatically repel each other and a decrease in the total amount and surface coverage of titania are observed. At a pH close to the IEP of titania (pH ~ 6) titania starts to agglomerate into larger aggregates due to the absence of electrostatic repulsion. The carboxylate anions are likely still present at this pH, as the isoelectric point for various succinylated biomacromolecules are in the pH = 4–7 range.[54,55] At lower pH, titania becomes positively charged and forms smaller aggregates while the succinic acid functionality is neutral. At acidic pH more titania will bind to the fibers as protonated carboxylic acids have been found to have a higher affinity for titania than un-protonated carboxylic acids.[56,57] This enhanced binding coupled with the smaller aggregates sizes lead to increased surface coverage of titania in electrospun fiber mats loaded at acidic pH.

Electrospun fibers mats loaded at different pH were tested for MC-LR degradation. Solar light degradation is shown in Fig. 9

Table 4 Average diameter of titania aggregates in aqueous solutions at different pH as determined by DLS

Titania type	P25			Kronos			$NF–TiO_2$		
pH	2	6	10	2	6	10	2	6	10
Diameter (nm)	127 ± 26	690 ± 97	400 ± 425	450 ± 20	1220 ± 40	1420 ± 30	930 ± 540	1400 ± 770	390 ± 90

Table 5 Surface Ti/C ratio (as determined using XPS) and percentage of titania in the fiber mats (as determined using a Ti-assay described in the Experimental section) for fibers electrospun from 80% acetic acid loaded with titania at different pH values. Each experiment was repeated three times on three separately made samples

	P-25			Kronos			$NF–TiO_2$		
	pH = 2	pH = 6	pH = 10	pH = 2	pH = 6	pH = 10	pH = 2	pH = 6	pH = 10
Surface Ti/C ratio	1.0 ± 0.2	0.5 ± 0.4	0.2 ± 0.1	0.5 ± 0.2	0.30 ± 0.05	0.21 ± 0.07	0.16 ± 0.07	0.03 ± 0.01	0.03 ± 0.01
TiO_2%	15 ± 3%	10 ± 1%	7.8 ± 0.2%	13 ± 1%	6 ± 1%	9.5 ± 0.1%	10 ± 0.7%	20 ± 8%	7.6 ± 0.4%

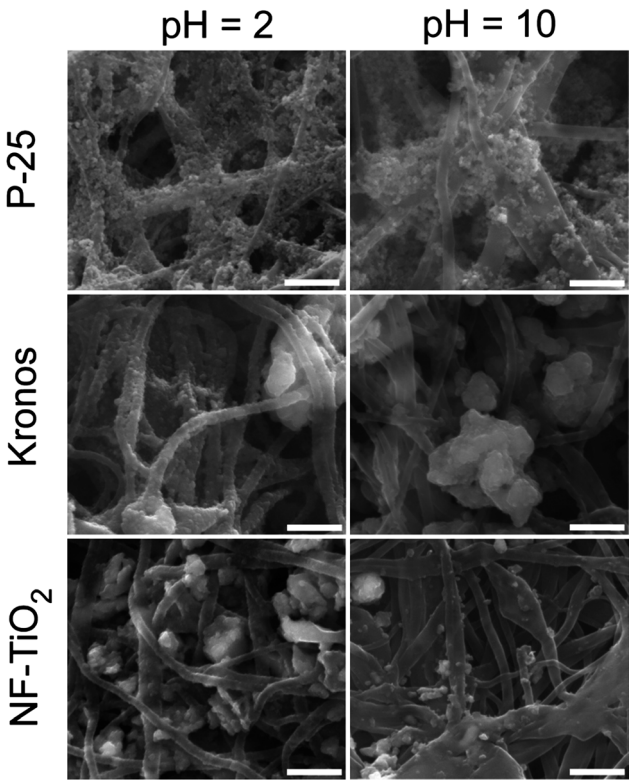

Fig. 7 SEM images of succinylated cellulose nanofibers formed at pH of 2 and 10 loaded with P-25, Kronos, and $NF–TiO_2$. All scale bars equal 1 μm.

and visible light degradation shown in Fig. 10. Under solar light, Kronos and P-25 titania degrade MC-LR completely for fibers loaded with titania at pH = 2 and 6. For fiber mats loaded at basic pH, P-25 based fiber mats still show sufficient MC-LR

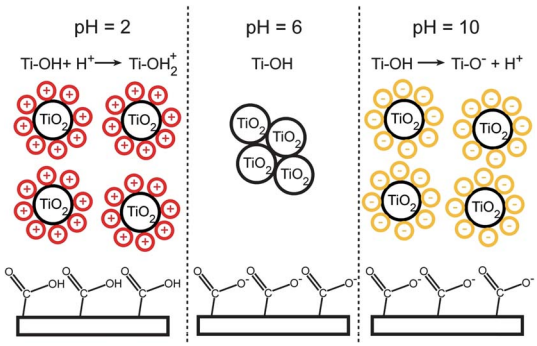

Fig. 8 Schematic depicting the surface chemistry, aggregation state and fiber chemistry at pH = 2, 6, and 10.

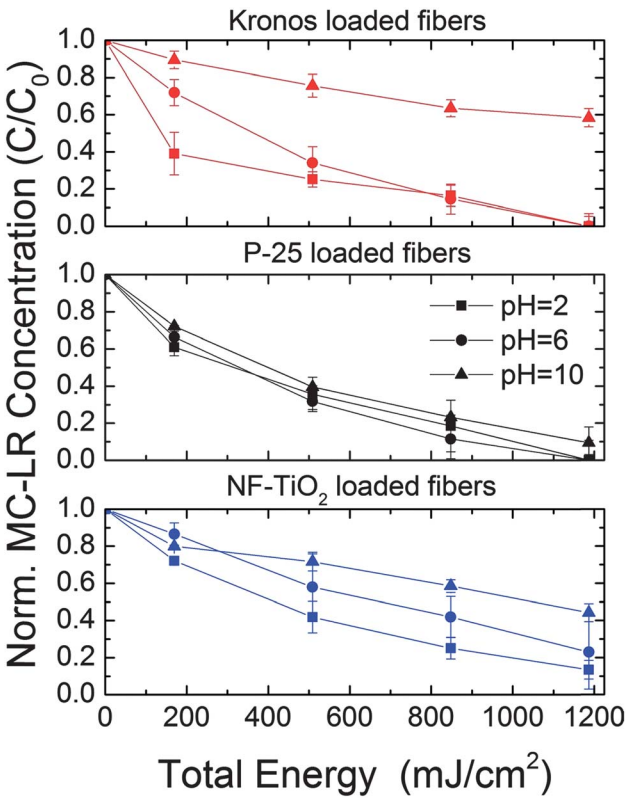

Fig. 9 Photocatalytic degradation of MC-LR under solar light conditions (average light intensity of 47.1 mW cm^{-2}) for Kronos loaded fibers (red lines), $NF–TiO_2$ loaded fibers (blue lines), and P-25 (black lines) at pH = 2 (squares), pH = 6 (circles), and pH = 10 (triangles).

degradation, while Kronos loaded fiber mats at a basic loading pH show a reduced amount of MC-LR degradation compared to acidic and near neutral loading pH. Data from Table 4 and Fig. 7 show that at pH = 10, P-25 aggregates are ~1/3 the size of Kronos. As such, more titania surface is exposed and thus a large amount of MC-LR is degraded. For electrospun fiber mats loaded with $NF–TiO_2$ nanoparticles, there are notable different in MC-LR degradation *vs.* loading pH. At a loading pH of 2, the $NF–TiO_2$ loaded fibers exhibit improved MC-LR degradation. This can be attributed to the relatively higher titania surface coverage compared to samples loaded at pH of 6 and 10 (Table 5). This effectively illustrates the importance of loading pH of titania onto fibrous substrates. Electrospun fiber mats loaded at pH = 6 show improved MC-LR degradation properties compared to fiber mats loaded at pH = 10 despite the identical titania surface coverage. However, there is a two-fold increase in the total amount of titania in the fibers loaded at pH = 6 *vs.*

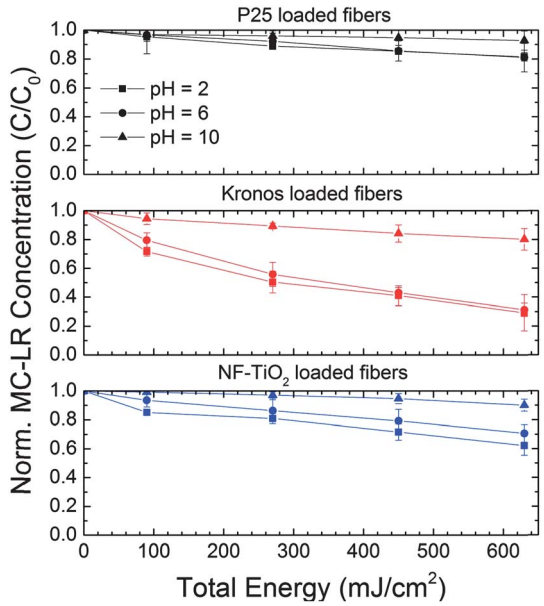

Fig. 10 Photocatalytic degradation of MC-LR under visible light conditions (average light intensity of 25 mW cm^{-2}) for P-25 (black lines), Kronos loaded fibers (red lines), and NF–TiO_2 loaded fibers (blue lines) at pH = 2 (squares), pH = 6 (circles), and pH = 10 (triangles).

pH = 10. For fibers loaded with P-25, the lack of change in photocatalytic activity at varying loading pH may be attributed to both the small nanoparticle cluster sizes and P-25's more efficient use of UV light compared to Kronos and NF–TiO_2. Visible light degradation of MC-LR exhibits similar trends with samples loaded at varying pH yet with an overall decrease in the amount of MC-LR degradation, with the exception of samples loaded with visible light inactive P-25.

Conclusions

Photocatalytic cellulosic fibers were made from electrospun fibers by a simple titania surface loading technique using UV and visible light activated titania nanoparticles. These photocatalytically viable fiber mats were tested for potential usage as decontamination membranes for the degradation of MC-LR, a potent cyanobacteria toxin. Surface area, titania surface coverage, and overall titania concentration for the electrospun fibers were correlated to MC-LR degradation. The surface coverage of titania and fiber mat surface area are more crucial to effective MC-LR degradation than the overall amount of titania in the fibers. These photocatalytic non-woven high surface area membranes could be advantageously employed for drinking water and waste water treatment applications using solar light as a renewable source of energy.

Acknowledgements

This work was supported in part by the Air Force Research Laboratory, Dayton Area Graduate Studies Institute (fellowship # RX09-7), the National Science Foundation (US-Ireland Collaborative Research, CBET 1033317) and the Cyprus Research Promotion Foundation through Desmi 2009–2010 which is co-funded by the Republic of Cyprus and the European Regional Development Fund (NEA IPODOMI/STRATH/0308/09). The authors would like to thank Linda Kasten (AFRL) for assistance with XPS experiments.

References

1 E. B. Kujawinski, M. C. Kido Soule, D. L. Valentine, A. K. Boysen, K. Longnecker and M. C. Redmond, *Environ. Sci. Technol.*, 2011, **45**, 1298–1306.
2 A. Wise, K. O'Brien and T. Woodruff, *Environ. Sci. Technol.*, 2011, **45**, 51–60.
3 E. Hoh, L. Zhu and R. A. Hites, *Environ. Sci. Technol.*, 2006, **40**, 1184–1189.
4 M. Wekler and C. Steinberg, *Environ. Sci. Technol.*, 2000, **34**, 3415–3419.
5 S. Di Pasqule, M. Paniconi, B. Aurichhio, L. Orefice, A. C. Schultz and D. De Medici, *J. Virol. Methods*, 2010, **165**, 57–63.
6 K. Lemarchand and P. Lebaron, *FEMS Microbiol. Lett.*, 2003, **218**, 203–209.
7 D. Bahnemann, *Sol. Energy*, 2004, **77**, 445–459.
8 H. Choi, E. Stathatos and D. D. Dionysiou, *Desalination*, 2007, **202**, 199–206.
9 M. R. Hoffmann, S. T. Martin, W. Choi and D. W. Bahnemann, *Chem. Rev.*, 1995, **95**, 69–96.
10 J. H. Braun, A. Baidins and R. E. Marganski, *Prog. Org. Coat.*, 1992, **20**, 105–138.
11 M. Grätzel, *Acc. Chem. Res.*, 2009, **42**, 1788–1798.
12 U. I. Gaya and A. H. Abdullah, *J. Photochem. Photobiol., C*, 2008, **9**, 1–12.
13 K. Schilling, B. Bradford, D. Castelli, E. Dufour, J. F. Nash, W. Pape, S. Schulte, I. Tooley, J. van den Bosch and F. Schellauf, *Photochem. Photobiol. Sci.*, 2010, **9**, 495–509.
14 X. Zhao, Q. Zhao, J. Yu and B. Liu, *J. Non-Cryst. Solids*, 2008, **354**, 1424–1430.
15 R. Molinari, M. Mungari, E. Drioli, A. Di Paola, V. Loddo, L. Palmisano and M. Schiavello, *Catal. Today*, 2000, **55**, 71–78.
16 T. Rajh, L. X. Chen, K. Lukas, T. Liu, M. C. Thurnauer and D. M. Tiede, *J. Phys. Chem. B*, 2002, **106**, 10543–10552.
17 Z. Wang, W. Mao, H. Chen, F. Zhang, X. Fan and G. Qian, *Catal. Commun.*, 2006, **7**, 518–522.
18 W. Kim, T. Tachikawa, T. Majima, C. Li, H.-J. Kim and W. Choi, *Energy Environ. Sci.*, 2010, **3**, 1789–1795.
19 W. Choi, A. Termin and M. R. Hoffman, *J. Phys. Chem.*, 1994, **98**, 13669–13679.
20 S. Klosek and D. Raftery, *J. Phys. Chem. B*, 2001, **105**, 2815–2819.
21 S. Kim, S.-J. Hwang and W. Choi, *J. Phys. Chem. B*, 2005, **109**, 24260–24267.
22 J. Zhang, Y. Wu, M. Xing, S. A. K. Leghari and S. Sajjad, *Energy Environ. Sci.*, 2010, **3**, 715–726.
23 M. Pelaez, A. A. de la Cruz, E. Stathatos, P. Falaras and D. D. Dionysiou, *Catal. Today*, 2009, **144**, 19–25.
24 R. Bacca, J. Kiwi, T. Ohno, P. Albers and V. Nadtochenko, *J. Phys. Chem. B*, 2005, **109**, 5994–6003.
25 X. Chen, Y. Lou, A. C. S. Samia, C. Burde and J. L. Gole, *Adv. Funct. Mater.*, 2005, **15**, 41–49.
26 S. In, A. H. Kean, A. Orlov, M. S. Tikhov and R. M. Lambert, *Energy Environ. Sci.*, 2009, **2**, 1277–1279.
27 Y. Choi, T. Umebayashi and M. Yoshikawa, *J. Mater. Sci.*, 2004, **39**, 1837–1839.
28 C. Han, M. Pelaez, V. Likodimos, A. G. Kontos, P. Falaras, K. O'Shea and D. D. Dionysiou, *Appl. Catal., B*, 2011, **107**, 77–87.
29 N. Shi, X. Li, T. Fan, H. Zhou, J. Ding, D. Zhang and H. Zhu, *Energy Environ. Sci.*, 2011, **4**, 172–180.
30 D. Klemm, B. Heublein, H.-P. Fink and A. Bohn, *Angew. Chem., Int. Ed.*, 2005, **44**, 3358–3393.
31 T. Yuranova, D. Laub and J. Kiwi, *Catal. Today*, 2007, **122**, 109–117.
32 M. J. Uddin, F. Cesano, D. Scarano, F. Bonino, G. Agostini, G. Spoto, S. Bordiga and A. Zecchina, *J. Photochem. Photobiol., A*, 2008, **199**, 64–72.
33 N. Abidi, L. Cabrales and E. Hequet, *ACS Appl. Mater. Interfaces*, 2009, **1**, 2141–2146.
34 S. Agarwal, A. Greiner and J. H. Wendorff, *Adv. Funct. Mater.*, 2009, **19**, 2863–2879.
35 D. Li and Y. Xia, *Adv. Mater.*, 2004, **16**, 1151–1170.

36 D. Li and Y. Xia, *Nano Lett.*, 2003, **3**, 555–560.
37 A. K. Alves, F. A. Berutti, F. J. Clemens, T. Graule and C. P. Bergmann, *Mater. Res. Bull.*, 2009, **44**, 312–317.
38 S. Zhan, D. Chen, X. Jiao and C. Tao, *J. Phys. Chem. B*, 2006, **110**, 11199–11204.
39 J. A. Lee, K. C. Krogman, M. Ma, R. M. Hill, P. T. Hammond and G. C. Rutledge, *Adv. Mater.*, 2009, **21**, 1252–1256.
40 J. A. Lee, Y. S. Nam, G. C. Rutledge and P. T. Hammond, *Adv. Funct. Mater.*, 2010, **20**, 2424–2429.
41 N. M. Bedford and A. J. Steckl, *ACS Appl. Mater. Interfaces*, 2010, **2**, 2448–2455.
42 M. G. Antoniou, A. A. de la Cruz and D. D. Dionysiou, *J. Environ. Eng.*, 2005, **51**, 1239–1243.
43 I. R. Falconer, *Environ. Toxicol.*, 1999, **14**, 5–12.
44 S. O. Han, J. H. Youk, K. D. Min, Y. O. Kang and W. H. Park, *Mater. Lett.*, 2008, **62**, 759–762.
45 W. A. Daoud, S. K. Leung, W. S. Tung, J. H. Xin, K. Cheuk and K. Qi, *Chem. Mater.*, 2008, **20**, 1242–1244.
46 H. Atwater, *Mater. Res. Soc. Bull.*, 2011, **36**, 57–62.
47 M. G. Antoniou, J. A. Shoemaker, A. A. de la Cruz and D. D. Dionysiou, *Toxicon*, 2008, **51**, 1103–1118.
48 H. Sedaira, K. A. Idriss and M. S. Abdel-Aziz, *Analyst*, 1996, **121**, 1079–1084.
49 K. T. Meilert, D. Laub and J. Kiwi, *J. Mol. Catal. A: Chem.*, 2005, **237**, 101–108.
50 S. Köhler, T. Liebert, M. Schöbitz, J. Schaller, F. Meister, W. Günther and T. Heinze, *Macromol. Rapid Commun.*, 2007, **28**, 2311–2317.
51 C. F. Liu, R. C. Sun, A. P. Zhang, J. L. Ren, X. A. Wang, M. H. Qing, Z. N. Chao and W. Luo, *Carbohydr. Res.*, 2007, **342**, 919–926.
52 K. Suttiponparnit, J. Jiang, M. Sahu, S. Suvachittanont, T. Charinpanitkul and P. Biswas, *Nanoscale Res. Lett.*, 2001, **6**, 27.
53 J. Jiang, G. Oberdörster and P. Biswas, *J. Nanopart. Res.*, 2009, **11**, 77–89.
54 E. K.-W. Toh, H.-Y. Chen, Y.-L. Lo, S.-J. Huang and L.-F. Wang, *Nanomed: Nanotechnol. Biol. Med.*, 2001, **7**, 174–183.
55 H. N. Ong, B. Arumugam and S. Tayyab, *J. Biochem.*, 2009, **146**, 895–904.
56 Y.-X. Weng, L. Li, Y. Liu, L. Wang and G.-Z. Yang, *J. Phys. Chem. B*, 2003, **107**, 4356–4363.
57 A. Vittadini, A. Selloni, F. P. Rotzinger and M. Grätzel, *J. Phys. Chem. B*, 2000, **104**, 1300–1306.

